Comparison of Conventional and Collapsed Region Operation of Capacitive Micromachined Ultrasonic Transducers

Yongli Huang, *Student Member, IEEE*, Edward Hæggström, Baris Bayram, *Student Member, IEEE*, Xuefeng Zhuang, *Student Member, IEEE*, Arif Sanlı Ergun, *Member, IEEE*, Ching-Hsiang Cheng, and Butrus T. Khuri-Yakub, *Fellow, IEEE*

***Abstract*—We report experimental results from a comparative study on collapsed region and conventional region operation of capacitive micromachined ultrasonic transducers (CMUTs) fabricated with a wafer bonding technique. Using ultrasonic pulse-echo and pitch-catch measurements, we characterized single elements of 1-D CMUT arrays operating in oil. The experimental results from this study agreed with the simulation results: a CMUT operating in the collapsed region produced a higher maximum output pressure than a CMUT operated in the conventional region at 90% of its collapse voltage (3 kPa/V vs. 16.1 kPa/V at 2.3 MHz). While the pulse-echo fractional bandwidth (126%) was higher in the collapsed region operation than in the conventional operation (117%), the pulse-echo amplitude in collapsed region operation was 11 dB higher than in conventional region operation. Furthermore, within the range of tested bias voltages, the output pressure monotonously increased with increased bias during collapsed region operation. It was also found that in the conventional mode, short AC pulses (larger than the collapse voltage) could be applied without collapsing the membranes. Finally, while no significant difference was observed in reflectivity of the CMUT face between the two regions of operation, hysteretic behavior of the devices was identified in the collapsed region operation.**

I. Introduction

As an attractive alternative to lead-zirconate-titanate (PZT) transducers for ultrasonic applications, capacitive micromachined ultrasonic transducers (CMUTs) have been developed for more than a decade [1]–[6]. Two common criteria used for evaluating transducers are bandwidth and sensitivity. Often, these characteristics can be exchanged during the design process. A commonly used figure of merit for ultrasonic transducers is the product of their bandwidth and their sensitivity/transmission efficiency [7]. Transducer development effort can, therefore, be based on maximizing this product, constrained by demands on size, cost, etc. From simplified physical models of the device, it is possible to understand what parameters provide sensitivity or bandwidth separately for CMUTs [8]–[10]. It is more difficult to see what parameters optimize the sensitivity-bandwidth product. Such optimization is usually carried out using a finite element method (FEM) approach [11], [12].

The sensitivity bandwidth product of a device can be maximized by using either an optimal signal [13] or an optimal physical design [12]. Besides optimizing the structure and geometry of the device, it is also possible to operate the transducer in a non-classical way [14], [15] to gain sensitivity or bandwidth. The sensitivity-bandwidth product can be increased either by increasing both factors or by increasing only one factor, e.g., the sensitivity, without sacrificing bandwidth. We characterized the CMUT operation of immersed devices experimentally at bias points ranging from zero volts to breakdown voltage, and found two stable regions of operation, as predicted in [14]. In this paper, we report the experimental results from operating CMUTs [6], [16], [17] in the collapsed region [14], [18], and compare those results to conventional region operation [16] results.

Manuscript received December 18, 2004; accepted April 14, 2006. The authors acknowledge the financial support of the Office of Naval Research and the National Institutes of Health. Dr. Hæggström acknowledges the Wihuri Foundation and the Academy of Finland for financial support.

Y. Huang is with Kolo Technologies, Inc., San Jose, CA 95135 (e-mail: yongli@ kolotechnologies.com).

E. Hæggström the Electronics research unit, University of Helsinki, Helsinki, Finland.

B. Bayram, X. Zhuang, A. S. Ergun, C.-H. Cheng, and B. T. Khuri-Yakub are with the Edward L. Ginzton Laboratory, Stanford University, Stanford, CA 94305-4088.

Digital Object Identifier 10.1109/TUFFC.2006.125

II. Device Design and Fabrication

A. Design

The basic structure of a CMUT is a parallel plate capacitor with a rigid bottom electrode and a top electrode residing on or within a flexible membrane. The membrane is used to transmit or detect an acoustic wave in the adjacent medium [15]. The cross section of a CMUT cell is shown in Fig. 1. A DC bias voltage is applied between the electrodes to deflect the membrane to an optimum position for CMUT operation, usually with the goal of maximizing sensitivity and bandwidth. During transmission, an AC signal is applied to the transducer. The alternating electrostatic force between the top electrode and the bottom electrode actuates the membrane to deliver acoustic energy into the medium. During reception, the impinging acoustic wave vibrates the membrane, thus altering the capacitance between the two electrodes. An electronic circuit detects this capacitance change.

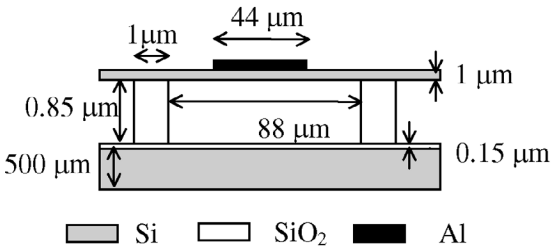

	Si	SiO_2	Al
Young's Modulus (GPa)	169	75	67.6
Poisson's Ratio	0.29	0.17	0.355
Density (kg/m^3)	2332	2200	2700
Relative Permittivity		3.78	

Fig. 1. The CMUT simulation model and material properties of the materials used in the simulations [22].

In order to enhance our understanding of collapsed region operation, the performance of the designed CMUTs was simulated by Ansys FEM software (ANSYS 5.7, Ansys, Inc., Canonsburg, PA). Each of the 580-μm by 5000-μm elements in the 1-D CMUT array consisted of hundreds of cells. Single-cell FEM calculations were combined with mask information about the array to predict the capacitance and average displacement as a function of bias voltage. For instance, the studied device design had 288 cells in the array element, with 0.06 pF/cell parasitic capacitance due to interconnects and configuration of the individual cells within the layout. The calculated parasitic capacitance was later taken into account when analyzing the data.

The CMUT cell in the FEM model featured a square silicon membrane supported on silicon oxide at its rim, with a process-induced tension less than 10 MPa. The membrane and the silicon oxide insulation layer on the substrate were separated by a vacuum gap. An aluminum electrode was positioned coaxially on the top surface of the silicon membrane center, as shown in Fig. 1.

The origin of this symmetric quasi-static 3-D FEM model [19] was at the center of the square membrane in the x-y plane. Modeling was therefore done only in the first quadrant (x, $y > 0$). Symmetry boundary conditions were applied on the x and y planes on either side of the model. The bottom of the substrate was clamped in all directions; thus, coupling into this substrate was neglected. The model and the meshing have been presented in [14]. One hundred divisions per membrane radius along the vertical dimension and two to six divisions along the horizontal dimensions were used. Because the gap was formed in a near vacuum condition during the wafer bonding, the top of the membrane was under the influence of 1 atm (atmosphere) pressure. While the top of the substrate constituted the ground electrode, the bottom of the silicon membrane (and not its top where the metal is located) acted as the hot electrode. Because the silicon is a semiconductor, the membrane acts as an electrical resistor at DC.

The ANSYS standard element types, SOLID122, which features charge and voltage variables, and SOLID45, which features displacement and force variables, were used in the electrostatic and structural analyses, respectively. The collapse of the membrane onto the substrate was modeled using surface-to-surface contact-target pair elements. These contact elements were used to detect contact between the membrane and the substrate surfaces. In order to re-mesh or re-morph the mesh inside the gap when the structure was collapsed, the surface elements were offset, defined as the bottom surface of the membrane and 0.006 μm above the insulation layer. Regarding remorphing and remeshing consult [20]. The contact elements used were TARGE170 and CONTA173. The augmented Lagrangian method was used to calculate the contact forces in this pair of contact-target elements. Surface friction forces were neglected. Neglecting friction constitutes a limitation associated with the use of these contact elements for modeling. The contact behavior of these surfaces was modeled using tabulated material properties of the contacting elements (silicon on the top membrane side and silicon oxide on the bottom insulation layer). These properties were needed to determine surface penetration and proximity [20].

The FEM analysis uses "nonlinear," large deformation calculations with stress stiffening for the structural analysis [20]. The nonlinear analysis takes care of geometrical nonlinearities. It is also capable of incorporating material nonlinearities if these properties are provided in a tabulated format. We did not use nonlinear material properties because relying on linear material properties sufficed to predict the behavior of the actual device. Due to the electrostatic-structural coupling, several iterations were performed until the structural energy and displacement converged to their respective values with a tolerance of 0.01%. The material definitions were based on linear material properties such as Young's modulus, Poisson's ratio, and density.

FEM was used to calculate the deformed membrane shape for any given bias voltage applied to the membrane electrode. When the applied voltage was close to the collapse voltage of the membrane, the electrostatic forces deformed the membrane to a great extent. As a consequence, these forces needed to be recalculated for the deformed membrane shape. The above steps were iterated until the equilibrium membrane deflection was reached. The predefined function ESSOLV [20] was used to solve this electrostatic-structural coupled model.

The convergence criterion for the simulation, which determined when the membrane was in its equilibrium position, was based on both the structural displacement and the electrostatic energy of the membrane. When equilib-

rium was reached, the predefined function CMATRIX [20] was used to extract the capacitance between the electrodes in the electrostatic analysis. In the structural analysis, membrane displacement data across the moving membrane area was used to calculate the average membrane displacement. Then, the bias voltage was incremented ("up" loop) or reduced ("down" loop) by 1% at each step. The new bias voltage was applied to the membrane in its current shape. This step reduced computation time and enabled us to study the hysteretic behavior of the transducer in collapsed region operation.

When the bias voltage was higher than the collapse voltage, the center of the membrane, with a certain contact area, collapsed onto the substrate. If the bias voltage was increased further, the contact area of the collapsed membrane increased [12]. When the bias voltage was decreased to a voltage larger than the snapback voltage, the contact area decreased and the membrane remained in contact with the substrate. The contact prevailed until the bias voltage was decreased below the snapback voltage. Therefore, after collapsing the membranes, reducing the voltage to a value between membrane collapse and snapback voltages maintained the membrane in contact with the substrate. Thus, in order to operate the CMUT in collapsed region, the DC bias voltage was initially increased above the collapse voltage. The bias voltage could then be set either lower or higher than the collapse voltage to achieve optimum performance.

The mechanical and electrical material properties used in the FEM calculations are shown in Fig. 1. The electrostatic analysis used the dielectric constant, and the structural analysis used Young's modulus, material density, and Poisson's ratio. The side length of the membrane was 88 μm, and its thickness was 1 μm. The membrane was separated by a 0.85-μm vacuum gap from the 0.15-μm-thick silicon oxide insulation layer. The side length of the aluminum electrode was 44 μm, and its thickness was 0.33 μm. Neighboring cavities were separated by a 1-μm-thick silicon oxide barrier.

Initially, only atmospheric pressure without bias voltage was applied to the membrane; its maximum deflection was predicted to be 0.43 μm. Collapse and snapback voltages for this membrane under atmospheric pressure were determined to be 50 V and 30 V, respectively. "Up"- and "down"-looping, starting from 10 V and 80 V, respectively, with a 1% change in bias voltage at each step, simulated the capacitance (CV) and average displacement (DV) as a function of the bias voltage. Finally, we investigated the impact of variations in cavity radius, the parameter that suffers from the largest variations during processing, on collapse voltage.

B. Fabrication

The CMUT arrays analyzed in this paper were fabricated using a wafer bonding technique [15]. In this bonding technique, the transducer membrane and cavity were defined on a silicon-on-insulator (SOI) wafer and on a prime wafer, respectively. Using silicon direct bonding in vacuum, the two wafers were bonded together to form a transducer. Because the membrane was made of single crystal silicon, it was possible to predict and control the mechanical properties of the membrane. The advantages of this bonding technique allowed for repeatable fabrication of CMUTs featuring predictable center frequency, bandwidth, collapse voltage, and electromechanical coupling coefficient. Because it has tighter specifications than traditional CMUT technology [18], this wafer bonding technique produced transducers with greater sensitivity-bandwidth.

Wafer bonding requires two smooth surfaces. We used prime grade wafers with low average surface roughness for the SOI wafer (top electrode) and for the bottom electrode wafer. Fabricating CMUTs using the wafer bonding technique was a four-mask process, as shown in Fig. 2. The process started with a low resistivity, 0.008–0.02 Ω·cm, 4-inch N type $\langle 100 \rangle$ silicon wafer that would be the future bottom electrode. The first step (Step a) was to grow 0.95-μm silicon dioxide at 1100°C on the silicon wafer, prior to cavity definition. The oxide layer was patterned by means of photolithography (Mask 1) and etched with buffered oxide etch (BOE 6:1) that stops on the silicon surface (Step b). The cavity depth was, therefore, determined by the thickness of the oxide layer. After photoresist removal, another thermal oxide layer was grown (1500 Å, Step c) as an electrical isolation layer for the CMUT. The wafer was then ready for wafer bonding. Prior to bonding, the wafer surface was cleaned and activated: first, 20 minutes in Piranha (H_2SO_4:H_2O_2 4:1); then, 15 seconds in hydrofluoric acid (HF 50:1); finally, 5 minutes in RCA1 (NH_4OH:H_2O_2:H_2O 1:1:5).

Wafers were bonded using a commercial wafer bonder (EV501, EV Group) at 10^{-5} mbar vacuum, at a temperature of 150°C (Step d). The bonded wafers were then annealed at 1100°C for two hours in a dry O_2 environment to make the bond permanent. In order to form the membrane (Step e), the wafers were then ground and etched using potassium hydroxide (KOH) back to the box (oxide layer) of the SOI wafer. The box layer was removed with BOE 6:1, completing the membrane fabrication. In order to secure thorough bonding everywhere, the thin membranes were allowed to be pushed by the atmospheric pressure toward the posts, and a one-hour post-anneal (1100°C at 1 atm) was performed to improve the bond between the membrane and the thin posts. The active silicon layer was subsequently patterned by photolithography (Mask 2) and plasma etching (Step f) to open a channel through the top layers to contact the CMUT bottom electrode. Next, 3300 Å of Al was deposited by a metal sputter system, and patterned (Mask 3) to serve as the CMUT top electrode (Step g). The last clean room step (Mask 4) removed the active silicon between CMUT elements to ensure electrical isolation (Step h). The fabricated CMUTs carried 88-μm or 102-μm-square, 1-μm-thick, single crystal silicon membranes. Finally, the devices were epoxy-glued to a fiberglass PCB board, and wire bonded for the tests, as shown in Fig. 3. In Fig. 4, a WYCO profiler 3-D graph shows a CMUT membrane before and after collapse.

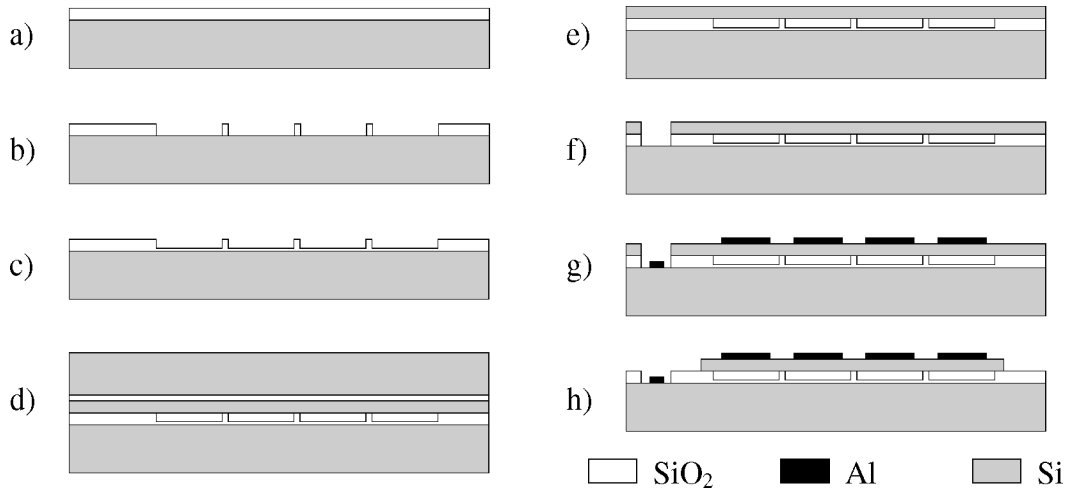

Fig. 2. Process flow in the fabrication of a CMUT with wafer bonding technology.

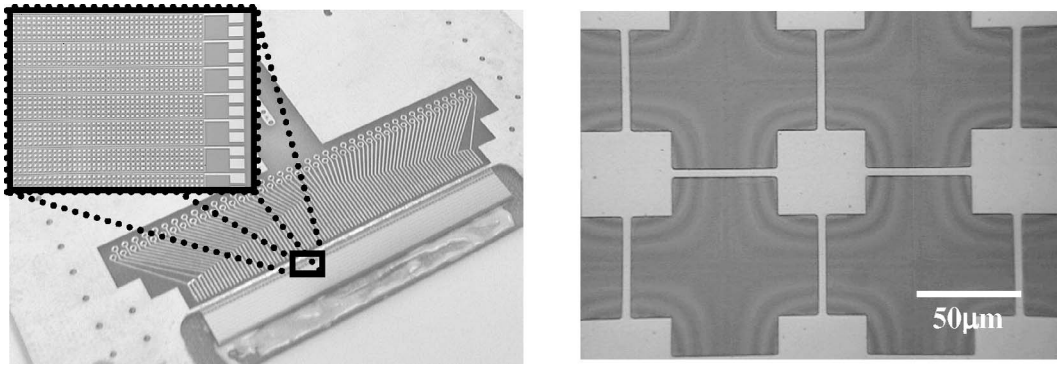

Fig. 3. Photographs of a device we used in the collapsed region tests. Left: This is a packaged 1-D, 86-element device with 288, 88-μm by 88-μm-square silicon membranes per element. The insert shows a 50X magnification of one of the elements. Right: Top view of the device with a 500X magnification.

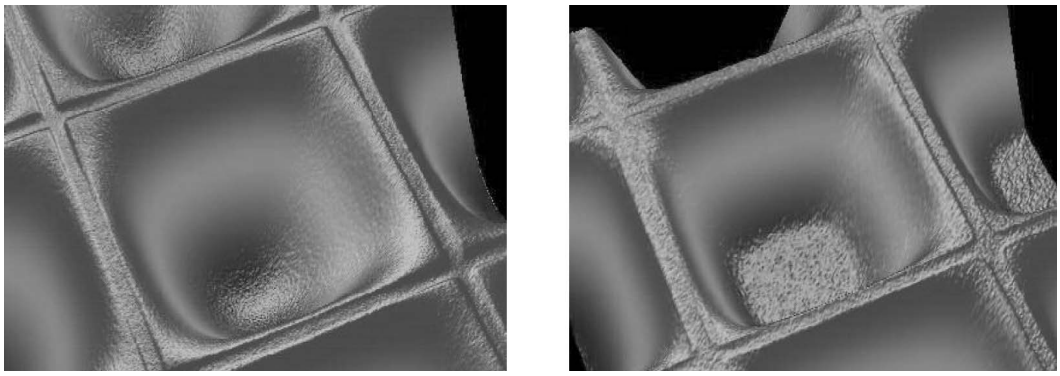

Fig. 4. Pictures of an 88-μm by 88-μm-square membrane before collapse (left) and after collapse (right) obtained by a WYCO profiler.

III. Device Characterization

The devices were characterized using capacitance measurements performed at 5 kHz, and using ultrasonic pitch-catch (PC) and pulse-echo (PE) measurements. In PC, both transmission properties and reception properties of the device operation were assessed. In all measurements, the amplitude or power of the received signal at the excitation frequency was deduced from its spectral content. All test data were measured from the 88-μm-square membrane CMUTs, except the corrected PE spectra and the reflection spectra, which were measured from the 102-μm-square membrane devices.

A. Capacitance Tests

An HP 33120A signal generator (Agilent Technologies, Inc., Palo Alto, CA) was used as the AC source in the measurements, except in the high voltage AC tests and the

reflectivity tests where a Panametrics 5058 pulser (Panametrics, Inc., Waltham, MA) was used. No buffer amplifiers were used either on the transmission or on the reception side. In the capacitance measurements, a DC source (Stanford Research Instruments PS-310, Stanford Research Systems Inc., Sunnyvale, CA) applied a negative DC bias on the CMUT, and a signal generator generated a 60-mV, 5-kHz AC signal (f). This frequency was chosen to obtain a "static-like" result with an AC measurement. An AC coupled oscilloscope (HP Infinium 500 MHz, Agilent Technologies, Inc.) with an input resistance of 1 MΩ (R_2) digitized the signal from a voltage divider consisting of a 130-kΩ (R_1) resistor and the CMUT. An average signal was calculated based on four consecutive data sets. The magnitude (m) of the Fourier transform of the smoothed signal was recorded in units of dBm. |Vout| was then computed according to $Vout = \sqrt{50 * 10^{(0.1*m-3)}}$ and the capacitance computed according to $C = \sqrt{(V\text{in}/V\text{out})^2 - (1 + R1/R2)^2}/(2\pi f R1)$. Seven measurements were performed during a time span of 72 hours of the CMUT element capacitance as a function of bias to determine the repeatability of the device behavior. The repeatability of device operation was characterized by the average coefficient of variation (standard deviation/mean, σ/μ) in the two regions.

The dynamic behavior of single membranes was investigated by means of laser vibrometry (LVM). However, this could not be done with traditional electrical impedance measurements that monitor only the average impedance of the membranes. By mounting the fiber-optic head of the LVM on a X-Y scanning stage, it was possible to probe several membranes of the devices to estimate the uniformity of the output of the fabrication process. LVM was used to measure the collapse voltage of 30 membranes to get an estimate for the sharpness of the transition from conventional to collapsed region of the devices. The sensor head, positioned coaxially with the membrane normal at a distance of 135 mm, was a Polytec OFV-1 (Polytec, Inc., Tustin, CA), and the controller was a Polytec OFV-3001. The vibrometer was used in displacement mode with a bandwidth of 20 MHz, a sensitivity of 1 V per 50 nm displacement, a spot size of 15 μm, and a displacement resolution of 1 pm [21].

The position of the LVM sensor head was controlled by a micrometer translation stage. The fiber-optic head was aligned for maximum reflected signal power. In both conventional region operation and collapsed region operation, the sensor head was scanned across each membrane until the maximum membrane displacement was observed on the oscilloscope. No standing waves from reflections off the 5-mm-in-diameter fiber-optic head were observed on the oscilloscope screen. No averaging was used. The maximum amplitude of the displacement signal was used to estimate the maximum deflection of the probed spot on the membrane.

The membranes were excited at their fundamental resonance frequency (f_0) with a continuous 0.1-V AC signal from the signal generator. The collapse of the membrane was determined from the power spectrum of the membrane motion. When the fundamental frequency abruptly changed, collapse was deemed to have taken place.

B. Ultrasonic Tests

In classical transmission pitch-catch measurements (TX), the distance between the hydrophone and the CMUT transmitter was 10.9 mm (Seki parameter, S = 1.13 [22]), and a 2.3-MHz sinusoidal wave train with 10–35 cycles and an amplitude of 0.5–2.5 V was applied to the CMUT. The hydrophone (PZT-Z44-0400, Specialty Engineering Associates, SEA, Sunnyvale, CA), with a −1 dB bandwidth of 1–11 MHz, was positioned by an Aerotech HDZ2 linear stage (Aerotech Inc., Pittsburgh, PA), with an accuracy of 1 μm. Before being read into the oscilloscope terminated with a 1-MΩ resistor and an 8-pF capacitor, the hydrophone signal was amplified by a 17-dB, 10 kHz–25 MHz, 50-Ω preamplifier. The hydrophone was scanned in the vertical plane so that a maximum reception voltage was obtained. The amplitude and nonlinear distortion of the received signal were measured as a function of DC bias voltage, and the amplitude of the received signal measured as a function of applied AC amplitude. The amount of nonlinear distortion was estimated by comparing the amplitude of the second harmonic (f_1) peak to that of the first harmonic (f_0) peak in the Hamming windowed power spectrum. A 5-V step function signal was applied to a CMUT that was DC-biased in the bandwidth measurement. The bandwidth was obtained from the frequency separation between the −3 dB points relative to the maximum point of the spectrum of the received signal.

A reception experiment was carried out to calculate the sensitivity of the CMUT. The experimental setup was the same as in the TX measurements, except that the hydrophone was replaced by a calibrated circular 12.5-mm-in-diameter unfocused Panametrics V109 transducer. In the reception pitch-catch measurement (RX), the distance between the PZT transducer and the CMUT was 86.1 mm (S = 2.51). Because it maximized the received signal, a 1.3-MHz, 0.5-V sinusoidal 35–50 cycle wave train was applied to the transmitting V109 transducer. The Aerotech translation stage positioned the transmitter, and the signal from the CMUT was read into the oscilloscope. The transmitter was scanned in the vertical plane until the maximum signal amplitude was received by the CMUT. In the procedure described above, measurements were made of the amplitude, bandwidth, and nonlinear distortion of the received signal as a function of bias voltage, and of the received signal amplitude as a function of applied AC amplitude.

In classical PE measurements, a 3-V, 10-MHz single-cycle square pulse (HP 33120A signal generator) was applied to the CMUT, together with a negative DC bias (Stanford Research Instruments PS-310). A polished aluminum block, placed at a 20.2-mm distance from the CMUT, was used as a reflector; the output signal from the CMUT was fed to the oscilloscope. Maximizing the amplitude of the received signal ensured parallelism between

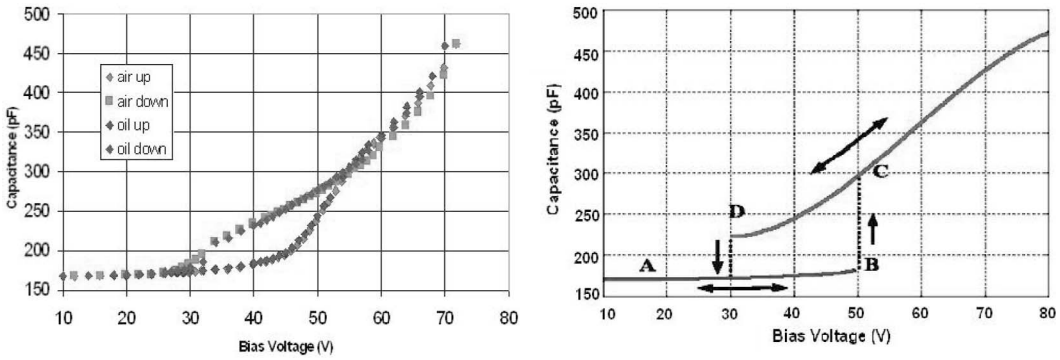

Fig. 5. The capacitance of a CMUT element as a function of bias, measured both in oil and in air (left) and simulated in air (right). "Up" indicates a measurement where the bias voltage was monotonously increased, whereas "down" indicates a measurement where the bias voltage was monotonously decreased. The parasitic capacitance in the experimental setup has been extracted.

the transducer and the reflector. In the manner described above, the amplitude and bandwidth of the received signal as a function of bias voltage were measured. The bandwidth was obtained from the frequency separation between the −6 dB points relative to the maximum point of the spectrum of the received signal.

In order to determine any disadvantage regarding triple transit echoes [23] from operating the transducer in collapsed mode as opposed to conventional mode, a PE was measured using a VP-1093 pinducer (Valpey Fisher Corp., Hopkinton, MA) as the source. A 200-V negative, 20-ns by duration, pulse was applied to the pinducer to probe the reflectivity of the CMUT surface. The needle transducer was 3 mm (S = 3) from the face of the CMUT. Again, the amplitude of the received signal was maximized. Since the pinducer suffered from ringing, the reflected signal was obtained by subtracting (in time domain) the signal obtained with the reflector present from the signal obtained when the reflector was removed. First, a 500-μm-thick polished Si wafer was insonified as a reference. Then the CMUT was measured using the same setup, first biased to conventional region, and then biased to collapsed region. The AC port of the CMUT was terminated either with a 50-Ω resistor or with a 130-kΩ resistor.

A certain amount of hysteresis in the device behavior was expected, due to contact forces between the membrane and the bottom electrode [24]. In an extensive study on the hysteresis of the CMUT, operating both in conventional region and collapsed region, the received signal amplitude was traced in the collapsed region of operation as a function of bias voltage, while alternately increasing or decreasing the DC voltage. Care was taken to ensure that the bias voltage alteration was always strictly increasing or strictly decreasing.

IV. Results

The predicted average capacitance and displacement curves of the devices exhibited two stable regions of operation, Figs. 5 (right) and 6 (right), respectively. One was the conventional region within which the bias voltage was below the collapse voltage of the CMUT (A-B); the other one was the collapsed region between the snapback voltage and the breakdown voltage of the CMUT (C-D) [14]. The static simulations predicted that it would be advantageous in terms of sensitivity and output pressure to operate the CMUT in the collapsed region. First, the capacitance change per applied voltage (6 pF/V) in this region is greater than in the conventional region (0.5 pF/V), resulting in higher reception sensitivity, Fig. 5 (right). Second, the average displacement per applied voltage in the collapsed region (25 Å/V) is greater than in the conventional region (20 Å/V), except when the bias voltage is close to collapse voltage (100 Å/V), at 90% of the collapse voltage, Fig. 6 (right). This static result, which parallels the result in [14], indicates that an improved capability to deliver energy into the surrounding medium might be achieved by operating the devices in the collapsed region as compared to the conventional region. However, this simulation cannot show the degree of improvement that is possible. Finally, in the conventional region, the CMUT was usually operated close to its collapse voltage to achieve optimal performance, i.e., maximizing sensitivity and bandwidth. However, the optimum bias voltage for collapsed region operation could be designed farther away from the collapse voltage than is possible in conventional region operation, allowing large AC signals to be used and, hence, generating a larger total dynamic range.

The loops of the capacitance-bias voltage (CV) curve in air and oil, Fig. 5 (left), show the repeatability of the device operation (σ/μ = 0.5% −1%). They also show three regions of operation: A) the conventional region; B) the transition region; and C) the collapsed region. The CV curve also shows a steeper slope in the collapsed region (C-D: 3–6 pF/V) than in the conventional region (A-B: 1 pF/V), indicating a potential for higher sensitivity. While the transition region (B-C) of the CV curve shows the steepest slope (12 pF/V), this slope is not infinite, due to the fact that different membranes in an element collapse at slightly different voltages, as evident in Fig. 7. Fig. 5 (left) shows a 10-V transition region in oil, which corresponded, according to our simulations, to a variation in cavity diameter of 3.6 μm, or less if the bonding was not ideal. The simulations also predicted that the transition region in snapback

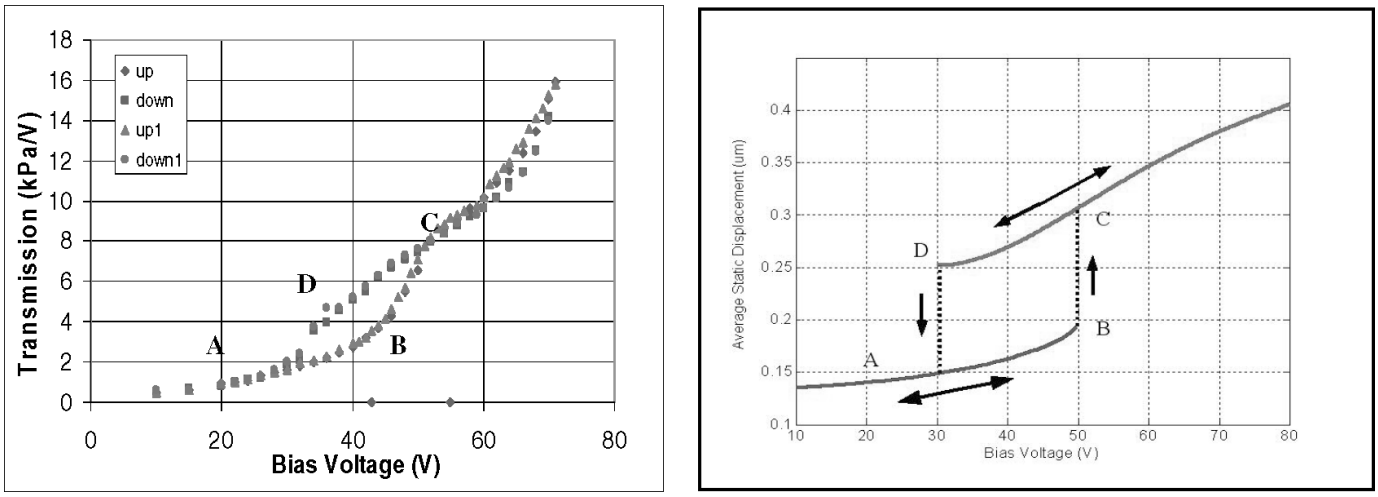

Fig. 6. The signal transmitted by an immersed CMUT element as a function of bias (left) and the simulated static displacement (right). The transducer was excited with a 2.5-V 35-cycle sinusoidal signal at 2.3 MHz. "Up" indicates a measurement where the bias voltage was monotonously increased, whereas "down" indicates a measurement where the bias voltage was monotonously decreased.

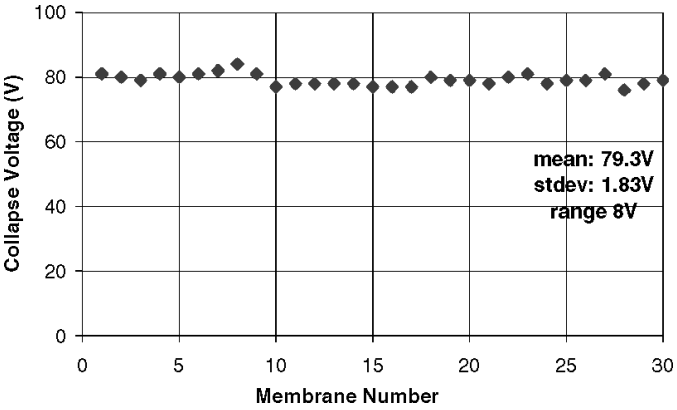

Fig. 7. Membrane collapse voltage measured in air by means of laser vibrometry from 30 membranes of the 288 membranes in an element.

(D-A) should be only 40% of the transition region at collapse, which is close to what can be seen in Fig. 5 (left).

We observed a high repeatability in these CV measurements. At any DC bias voltage, the maximum measured capacitance spread was 12.8 pF when increasing the bias ("up"), and 13.1 pF when decreasing the bias ("down") along the C-V curves. The maximum standard deviation across the whole range of bias voltages of the measured capacitance was 3.5 pF "up" and 4.3 pF "down". The average standard deviation was 0.8 pF ($\sigma/\mu = 0.5\%$) "up" and 1.7 pF "down" ($\sigma/\mu = 0.5\%$). These coefficients of variation should be compared to those in [25], which describe devices fabricated using the conventional technique, where a capacitance variation of 5.5% and a center frequency variation of 9.9% were reported. The corresponding average values for the conventional region were 1.29 pF ($\sigma/\mu = 0.74\%$) "up" and 1.68 pF "down" ($\sigma/\mu = 0.96\%$), and for the collapsed region 5.90 pF ($\sigma/\mu = 1.97\%$) "up" and 3.19 pF "down" ($\sigma/\mu = 1.28\%$). Between points B and C, the membranes collapsed. The width of the transition region (B-C) was 6 V. As mentioned above, we observed a finite slope in the C-V curve at the transition region. The maximum and minimum collapse voltages (measured with the laser vibrometer in air) were 84 V and 76 V, respectively, with a mean of 79.3 V, a standard deviation of 1.83 V, and a range of collapse voltages of 8 V, Fig. 7. At point C, Fig. 5 (left), the transition region ended, indicating that all of the membranes had collapsed. At point D, the slope of the C-V curve increased, indicating that the membranes had snapped back (D-A).

The two loops of the pitch-catch (TX, RX) curves, obtained with the CMUT transmitting and the hydrophone receiving, Fig. 6 (left), and vice versa in Fig. 8 (left), show that the repeatability of the devices observed in the air measurements carries over to the immersion measurements. These curves, again, exhibit the previously mentioned three regions of operation: they showed increased transmitted signals (TX), 94% increase, Fig. 6 (left), and received signals (RX), 80% increase, when the devices were operated in the collapsed region compared to the conventional region, Fig. 8 (left). The similarity in shape of the PE curve, Fig. 8 (right), to the TX and RX curves was expected, since PE is TX times RX, at least in principle. The PE curve shows that with a 50-V bias, a device working in the collapsed region gains 11 dB compared to pre-collapse region operation.

The region above the crossover point shows the largest signals. The collapse and snapback regions are visible. Because the membranes collapse and snap back at different voltages, the slopes of the curve in these regions are, again, not infinite.

The uncorrected TX fractional bandwidth (FBW) (∼120%) for a transmitting CMUT in pre-collapse region operation was lower (∼160%) than in the collapsed region, Fig. 9 (left). There is no clear trend for PE uncorrected FBW, Fig. 9 (right) as a function of the bias voltage. The FBW curve showed a broader fractional bandwidth (∼130%) in collapse, compared to that (∼120%) in con-

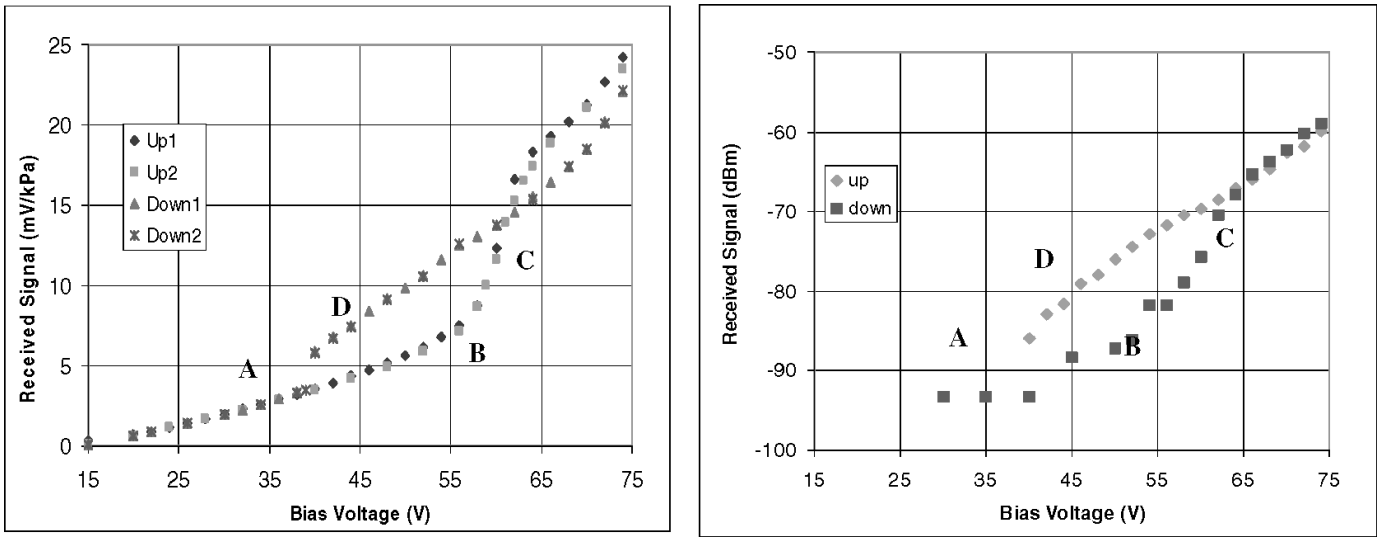

Fig. 8. The signal received by an immersed CMUT element as a function of bias (left) in pitch-catch and pulse-echo (right) measurements. "Up" indicates a measurement where the bias voltage was monotonously increased, whereas "down" indicates a measurement where the bias voltage was monotonously decreased. A 2-V 35-cycle sinusoidal signal at 1.3 MHz was applied to the PZT in the PC measurement.

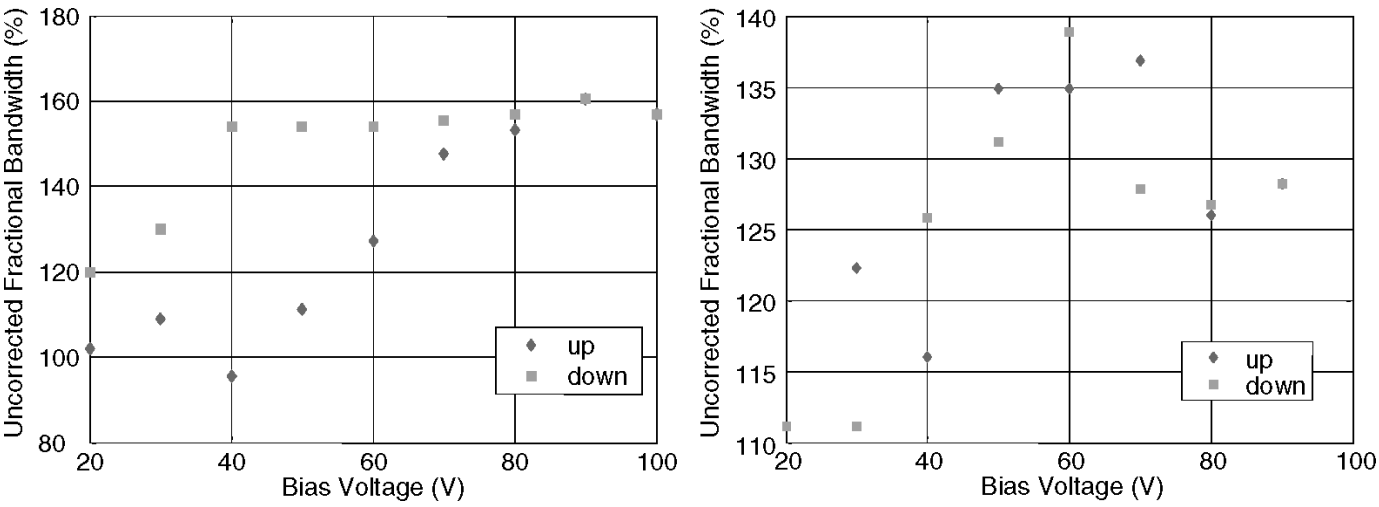

Fig. 9. Left: The −3 dB uncorrected fractional bandwidth of the signal transmitted (TX) by an immersed CMUT element as a function of bias in pitch-catch measurements. Right: The −6 dB uncorrected fractional bandwidth of the signal received in pulse echo (PE) by an immersed CMUT element as a function of bias. "Up" indicates a measurement where the bias voltage was monotonously increased, whereas "down" indicates a measurement where the bias voltage was monotonously decreased.

ventional region operation. However, both the center frequency and uncorrected absolute bandwidth (ABW) of a device operating in collapse region are higher than in the conventional region.

Fig. 10 shows the appearance of both the received signal and its bandwidth when the device is active in either region of operation. The gains, which originate from the shift of the high frequency −6 dB cut-off (3.9 MHz to 6.0 MHz), accrue both in absolute bandwidth (2.9 to 5.0 MHz) and in fractional bandwidth (from ∼120% to ∼140%).

The linearity of the CMUT in reception was determined during the RX measurements by altering the AC signal applied to the calibrated PZT transducer. The device linearity was characterized by the maximum deviation from a linear input-output behavior, and found to be lower than 0.7%. No apparent difference in linearity in reception was observed between conventional mode and collapsed mode operation, Fig. 11 (right).

The linearity of the devices for AC amplitudes below 16 V was determined during the TX measurements. In transmission, the full-scale linearity, i.e., the largest deviation from a line through the 0 V_{ac} and 16 V_{ac} data points, normalized by the value for 16 V_{ac}, was less than 4.5%. The advantage of operating the devices in collapsed region was seen from the larger signal produced with this mode of operation, compared to the signal produced in conventional mode operation, Fig. 11 (left). The measured improvement in full-scale linearity was low—0.1 percentage points.

During the large signal AC tests, it was found that these signals had little influence either on the center frequency or

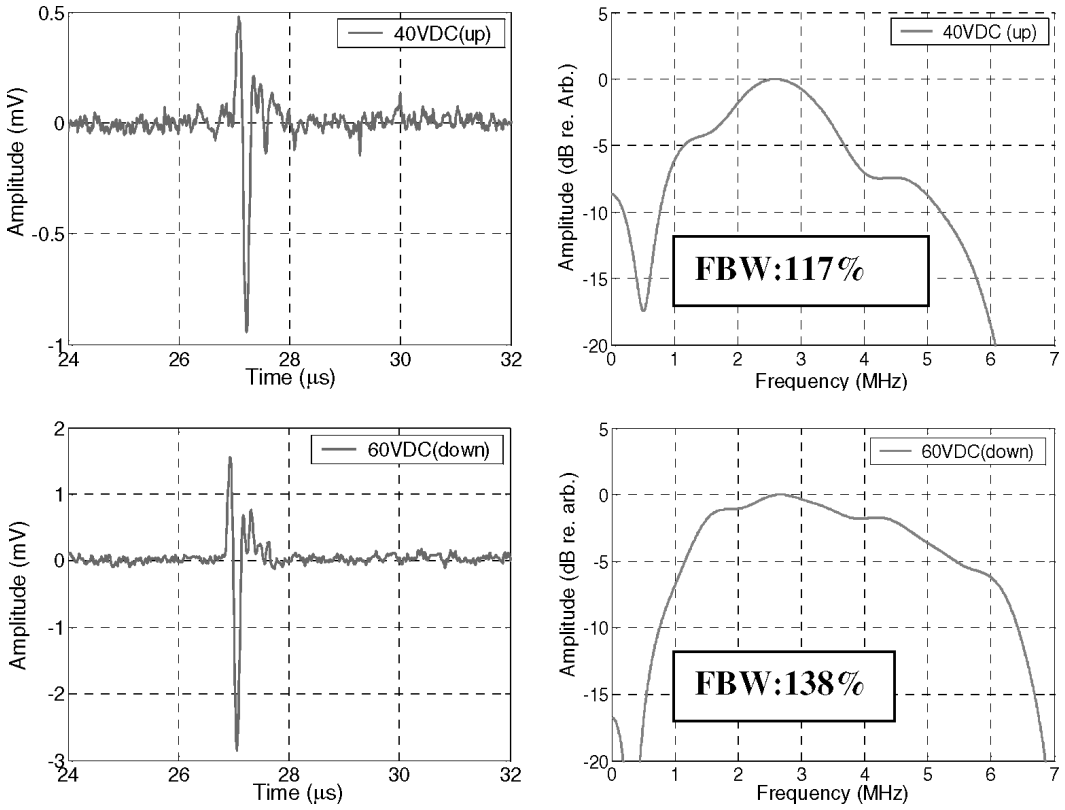

Fig. 10. The received PE signal (left) and corresponding amplitude spectrum (right) of the received signal. Upper results are from the pre-collapse region and lower results are from the collapsed region. The −6 dB uncorrected fractional bandwidth (FBW) is indicated. The transducer was excited with a single +3-V 10 MHz square pulse.

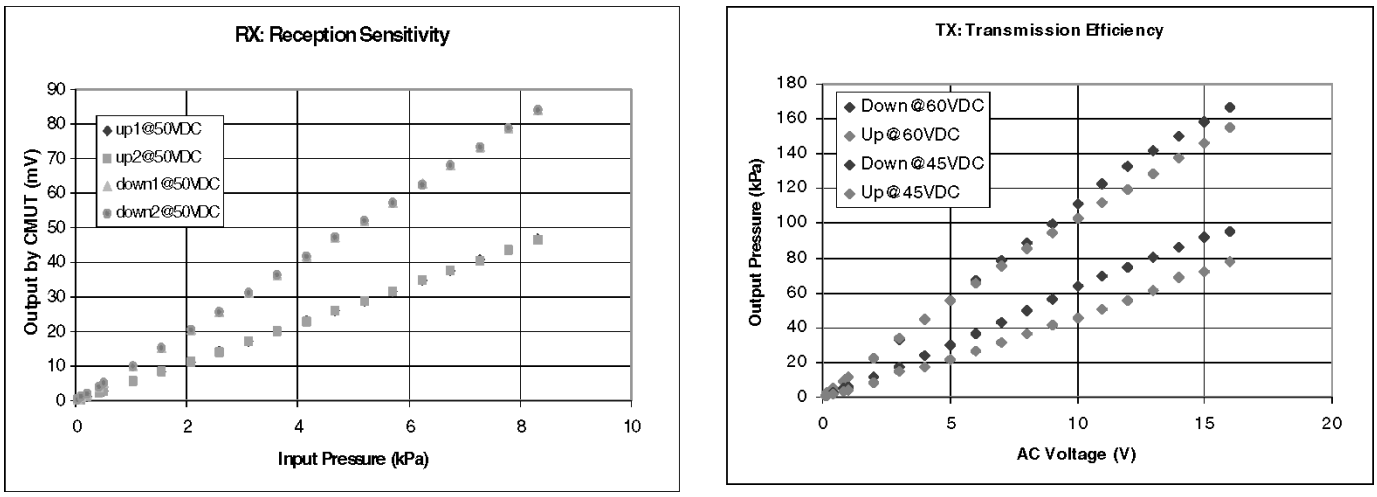

Fig. 11. Test of full-scale linearity. The 35-cycle sinusoidal signal transmitted by one CMUT element as a function of applied signal (left) and the signal received by a CMUT as a function of signal applied to a PZT transmitter (right). "Up" indicates the results from the pre-collapse region and "down" indicates the results from the collapsed region.

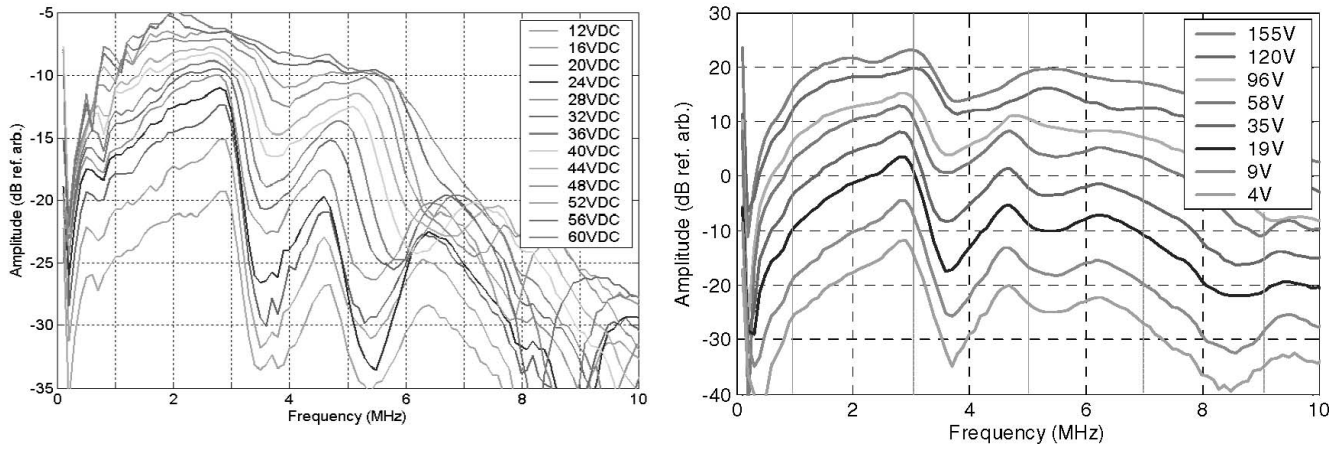

Fig. 12. Left: The frequency content of the transmitted 8-V step signal using various bias voltages. Right: The frequency content of the signal transmitted by a CMUT element as a function of the applied 20-ns negative spike at 24-V bias. The −3 dB fractional bandwidth at 155 Vac was 82% (1.95 MHz/2.37 MHz) for the CMUT in transmission.

on the bandwidth of the transducer, Fig. 12 (right). This implied that an AC signal, whose amplitude was much larger than the collapse voltage of the device, could be applied without collapsing the CMUT membranes in the conventional region. Thus, the oil loading was important for determining the dynamic response of an immersed membrane. For CMUTs with a collapse voltage of 50 V, the negative output pressure was 0.76 MPa at 3 MHz with 155 V_{ac} and 24 V_{dc}. This is, however, not an upper limit for the output, as the device design was not optimized for maximum output pressure. It is also noteworthy that the devices were not collapsed during the operation.

Nonlinear distortion in this investigation was defined as the ratio of power in the second harmonic to the power in the fundamental frequency of the TX or RX signal. From both experimental and simulation results of the CV, TX, and RX characteristics, a CMUT exhibits a nonlinear behavior as a function of input signal. Since the output pressure was different in conventional and collapsed region operation, the nonlinear generation in oil, which is dependent on the square of the output pressure, was also different [26]. We chose not to correct for this discrepancy, since the aim of this paper was to compare conventional and collapsed region operation of a CMUT, essentially keeping V_{ac} and V_{dc} constant. In Fig. 13, it is evident that the nonlinear distortion was higher in TX for a CMUT operating in the collapsed region. The nonlinear distortion also showed less bias dependence in collapsed region operation than in conventional region operation.

In the reflectivity tests, no apparent difference was seen between the reflected signals with the two different electrical loads. Nor was there any apparent difference, other than a dip in the spectrum, evident between the two modes of operation in the amplitude or the spectrum of the reflected signal. There was, however, a phase difference close to 180° between the reflections from a prime Si wafer and the CMUT face, Fig. 14 (left), implying that the impedance of the CMUT was lower than the impedance of oil, 1.42 MRayl [27]. Since the impedance of silicon is

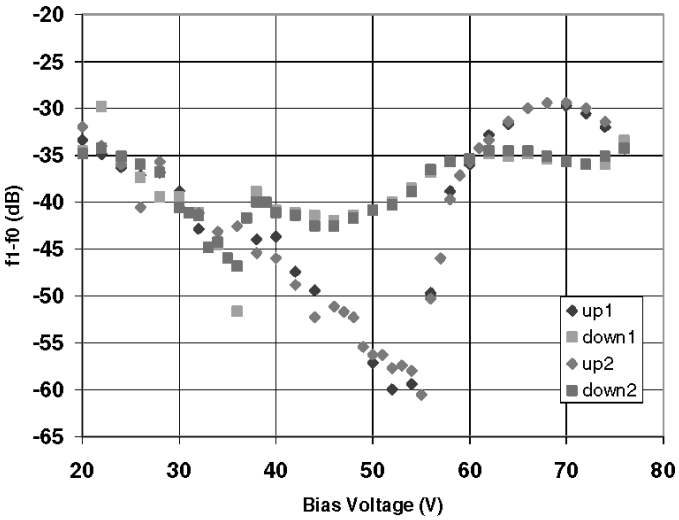

Fig. 13. The measured nonlinear content of the signal transmitted by the immersed CMUT element as a function of bias. The transducer was excited with a 2.5-V 35-cycle sinusoidal signal at 2.3 MHz. "Up" indicates a measurement where the bias voltage was monotonously increased, whereas "down" indicates a measurement where the bias voltage was monotonously decreased.

larger than that of oil, this result indicated that the dominating part of the reflection was from the vacuum cavity over which the membrane was suspended, and not from the silicon posts [22]. Moreover, the reflection from the CMUT was lower than from the prime silicon wafer, as evident in Fig. 14 (left). These two facts indicated that the reflection from the CMUT comprises two components of opposite phase: one from the vacuum cavity behind the silicon membrane, and one from the silicon posts. The total reflection was the sum of these components, with the reflection from the vacuum backing dominating.

The membrane was not acoustically completely invisible, since prior to entering the transition region there was a dip in the spectrum, Fig. 14 (right), at approximately 2.2 MHz, consistent with the edge seen in the PE

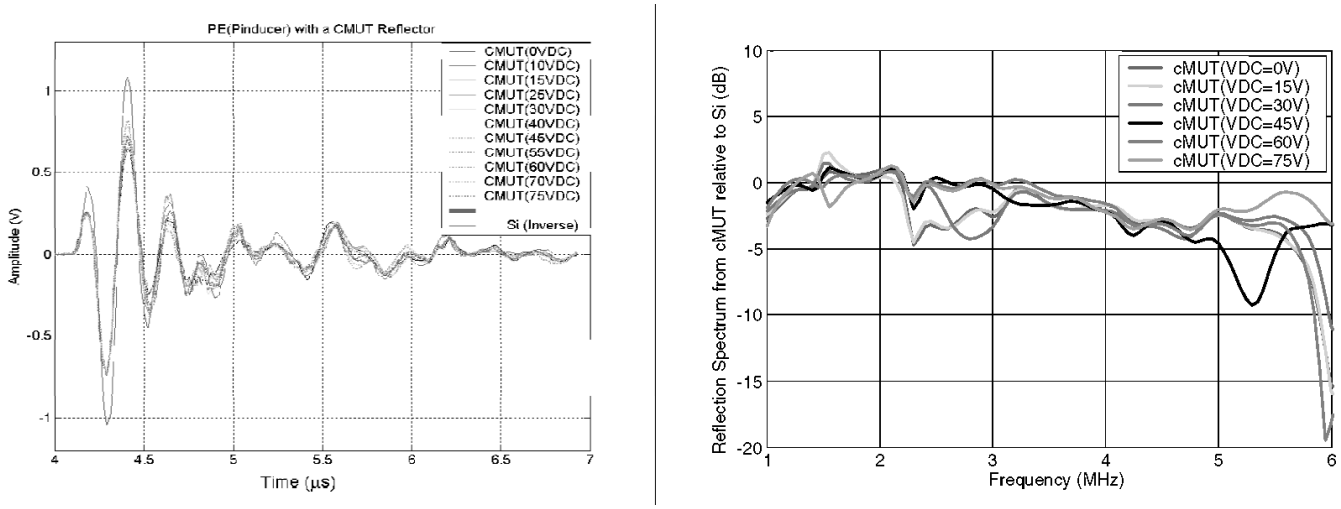

Fig. 14. Signal reflected off an immersed CMUT surface as a function of bias voltage together with the inverted signal reflected off a silicon wafer. Left: The transducer was excited with a −200 V signal of 20-ns duration. Right: Reflection spectra of the received signal calibrated with the Si wafer spectrum.

spectrum, Fig. 10. Neither the ridge, that did not vanish with increased distance to the membrane, nor the dip was present after the collapse of the membranes, indicating that the membranes contributed partly to the observed reflection.

The reflection from other reflectors such as posts and backings were fairly identical in both regions of operation. However, the small difference between the reflectivity of the CMUT surface in the two modes of operation supported the earlier conclusion that the vacuum behind the membranes dominated the reflection over the silicon parts of the device. All in all, no large disadvantage in increased inclination to triple transit echoes occurs when operating the CMUT in collapsed region compared to operating in conventional region.

The following results summarize the gains in ultrasonic performance of the CMUT obtained when using the collapsed region operation compared to the conventional region operation. It is again stressed that these devices were not optimized for either bandwidth or transmission efficiency/sensitivity.

In TX, the amplitude of the transmitted 50-cycle 2.3-MHz uncorrected signal increased by 94% at 45 V_{dc} (3.1 kPa to 6.0 kPa). Maximally, 16.1 kPa/V_{ac} was transmitted at 70 V_{dc}. The uncorrected bandwidth of the received one-cycle signal increased by 78% at 35 V_{dc}, becoming 2.01 MHz at 35 V_{dc}. The full-scale linearity of the devices increased by 0.1 percentage point. In RX, the amplitude of the received 50-cycle 1.3-MHz signal increased by 77% at 55 V_{dc}. Maximally, 24.2 mV/kPa was received at 74 V_{dc}, corresponding to 14.0 dB/kPa/$Hz^{0.5}$ into 58 kHz when the noise level was 20 μV_{pp}. The uncorrected bandwidth of the received one-cycle signal increased by 13% at 54 V_{dc}, becoming 1.06 MHz (82% fractional bandwidth) at 54 V_{dc}.

In PE, the amplitude of the received 50-cycle 2.3-MHz signal increased by 372% at 50 V_{dc}. Maximally, 0.4 mV/V_{ac} was received at 76 V_{dc}, corresponding to 34.4 dB/$Hz^{0.5}$ into 1.22 kHz when the noise level was 0.22 μV_{pp}. The absolute bandwidth of the received one-cycle sine signal increased by 158% at 40 V_{dc}. The largest measured absolute bandwidth was 4.9 MHz at 60 V_{dc}, corresponding to a 138% uncorrected (attenuation and diffraction) fractional bandwidth. The corrected fractional bandwidth was 140% at 45 V_{dc}.

In both transmission and reception, the deviation from linearity of the devices was less than 4.5%. The gains in transduction efficiency and fractional bandwidth come at the expense of a 5-dB increased harmonic distortion in TX. The overall nonlinear content was, however, below −30 dB when compared to f_0.

The hysteretic behavior of immersed devices was investigated in three regions: conventional, between collapse and snapback, and above collapse. These measurements were carried out either as "up-down tests", Figs. 6 (left) and 8 (left), to determine the maximum hysteresis, or as "spiral tests", Figs. 15 and 16, to identify what determines the amount of hysteresis observed. It was evident from Fig. 15 that the devices suffered from more hysteresis relative to full scale (13.7%, i.e., 0.46%/V_{dc}) when they were operated in collapsed mode than when they were operated in conventional mode (5.5%, i.e., 0.18%/V_{dc}). The hysteresis in the conventional region at low bias voltages was on a par with the measurement error. It was further evident that the maximum hysteresis observed depended on both the bias voltage, Fig. 16 (right), and on the bias range investigated, Fig. 15 (left, lower part of the curve).

For readability key device performance characteristics are presented in Table I.

V. Discussion

The difference between the experimental results and the simulation predictions was, in general, the abrupt change in capacitance and average displacement in the simula-

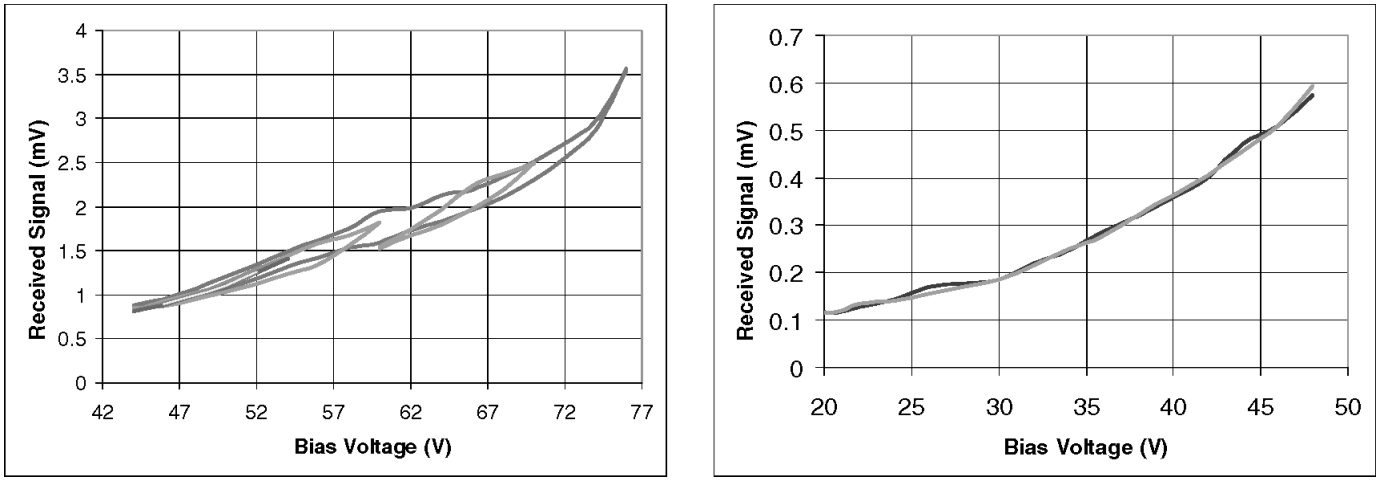

Fig. 15. Hysteresis is seen in an immersed CMUT dring transmission in collapsed region (left) but not during transmission in pre-collapse region (right). The collapsed region graph contains five loops used to investigate the impact of bias point and bias range selection on the hysteresis of the devices. A 0.5-V 30-cycle sinusoidal signal at 2.3 MHz was applied to the CMUT.

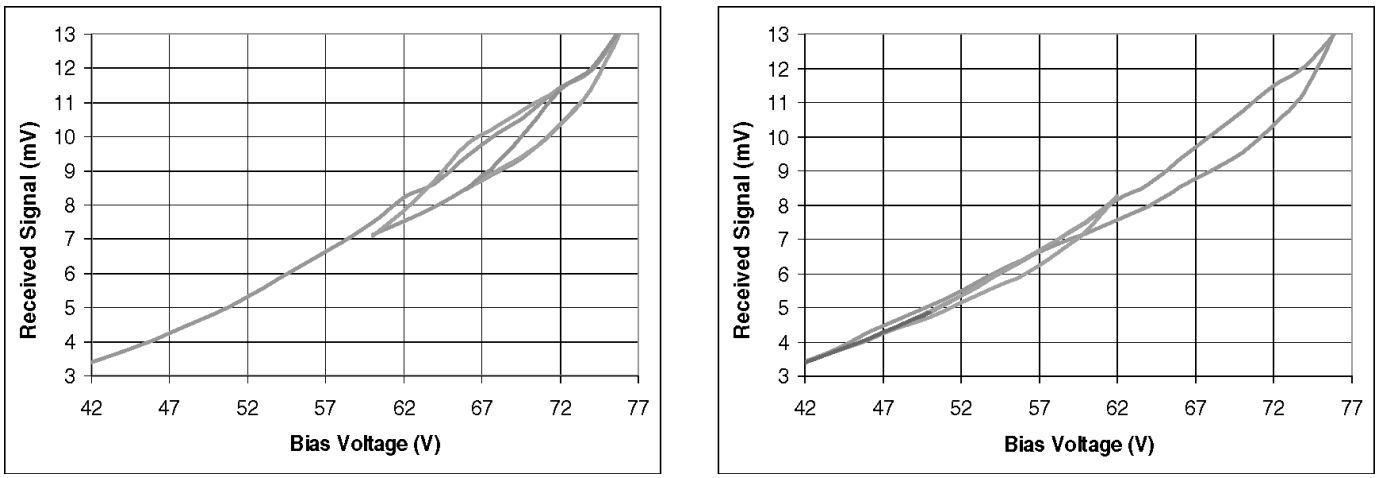

Fig. 16. Hysteresis in an immersed CMUT dring reception in collapsed region operation above collapse voltage (left) and between collapse and snapback voltages (right). A 2.5-V 30-cycle sinusoidal signal at 1.3 MHz was applied to the PZT.

tions at collapse and snapback, but not in the experimental results, Figs. 5, 6, and 8; the latter showed a change with a finite slope at these voltages. This discrepancy is explained by the population of CMUT cells that show a collapse voltage distribution, Fig. 7. The agreement in the collapse voltage between the laser vibrometer results and the capacitance results measured in air lent credibility to the predictions of the capacitive results measured in oil.

The derivative of the CV curve, Fig. 5 (left), was indicative of the TX curve, Fig. 6. The TX curve was, however, the result of an AC test, Fig. 6 (left); thus, the TX curve could not be compared directly to the derivative of the DV curve, Fig. 6 (right), because the membrane in the quasi-static DV case did not feel the reactive load of the immersion liquid. This load made it possible to apply a larger AC signal close to collapse voltage without collapsing the membrane, Fig. 12 (right), than the quasi-static modeling predicted. The deficiency of the FEM to predict the use of large AC signals without collapse is due to the fact that the modeling is static while the load is a dynamic.

The improvement in reception sensitivity gained by operating the device in collapsed mode was primarily due to the reduced inter-electrode separation that provided a steeper gradient in the electric field. The gain in output pressure was mainly due to stronger actuation forces as the electrode spacing was reduced. The advantage of using collapsed mode operation was larger in TX, Fig. 6 (left), than in RX, Fig. 8 (left), since the latter is proportional to d^{-1}, whereas the former is proportional to d^{-2}. In both cases, however, the collapsed mode operation was advantageous.

Comparing the bandwidth of CMUTs working in the conventional region with that of CMUTs in the collapsed region may shed light on the physics behind the device operation. This comparison is especially interesting, if, as here, an identical measurement setup is used in both cases. It is important to notice that the altered bandwidth still fit into the bandwidth of the amplifiers, and because both the center frequency and the bandwidth were different, the applicable absorption and diffraction corrections were different in the two cases. Using a filter analogue, we discuss

TABLE I
DEVICE CHARACTERISTICS.

TX	Efficiency @45 Vdc	Bandwidth @35 Vdc	Linearity deviation	Nonlinearity (f1-fo)	Hysteresis[1]
Pre-collapse	3.1 kPa/Vac	1.13 MHz	$<4.5\%$	<-35 dB	$<0.18\%$/Vdc
Collapsed	6.0 kPa/Vac	2.01 MHz	$<4.5\%$	<-40 dB	$<0.46\%$/Vdc
Advantage	94%	78%	+0.1% point	−5 dB	
Max	16.1 kPa/Vac @74 Vdc	160%@90 Vdc		−30 dB @30 Vdc	

RX	Efficiency @55 Vdc	Bandwidth @54 Vdc	Linearity deviation	Nonlinearity (f1-fo)	Hysteresis
Pre-collapse	7.1 mV/kPa	0.94 MHz	$<0.7\%$	***[2]	$<0.1\%$/Vdc
Collapsed	12.5 mV/kPa	1.06 MHz	$<0.7\%$	***	$<2\%$/Vdc
Advantage	77%	13%	0%		
Max	24.2 mV/kPa @ 74 Vdc				

PE	Efficiency @50 Vdc	Bandwidth @40 Vdc	Linearity deviation	Nonlinearity (f1-fo)	Hysteresis
Pre-collapse	−87.1 dBm	2.9 MHz (117%)	***	***	***
Collapsed	−75.7 dBM	4.6 MHz (126%)	***	***	***
Advantage	372%	158%			
Max	58.9 dBm@74 Vdc	138%@60 Vdc			

[1]Entries indicated (***) were not measured.
[2]The hysteresis was determined from the second up-down cycle as:
Hysteresis = {(max_signal_diff (up,down))/(max_signal-min_signal)}/(max_Vdc-min_Vdc).

the TX bandwidth results and the dissimilar relationship between bias voltage and capacitance, output power, and fractional bandwidth observed in the devices.

Both the TX and the PE results showed that operating the devices in the collapsed region indeed provided a larger fractional—as well as absolute—bandwidth than operating them in the conventional region, Figs. 10 and 12 (left). Hence, an increase in their fractional bandwidth was an important advantage gained by operating the devices in the collapsed region as compared to operating them in the conventional region.

At the high end of the bandwidth, the second harmonic mode determines the cut-off frequency of the particular CMUT tested, evidenced by the fact that the high-end spectral change is steeper than would be caused by attenuation and diffraction. Moreover, additional tests on devices with identical element size (and consequently identical attenuation and diffraction) but with different membrane size, showed that the rapid cut-off frequencies increased with decreasing membrane size. Hence, there is an absolute high-frequency limit for the upper corner frequency that depends on the size and geometry of the moving membrane. When the membrane collapses, both the first and the second harmonic modes abruptly shift to a higher frequency, as does the high frequency cut-off. If the bias voltage is increased, the corner cut-off frequency (−3 dB from the maximum at the high-frequency side) continues to shift gradually to higher frequencies, since the size of the moving part of the membrane decreases with bias in collapse, consult Fig. 12 (left). The factors that affect the FBW depend on the device design, too. For instance, if the second harmonic frequency is designed to be much higher than the upper 3-dB cut-off frequency, this corner frequency may be determined mainly by the frequency-dependent attenuation of the immersion medium. Another factor that may have an impact on the upper corner frequency is the total capacitance between the two electrodes, which acts like a low-pass filter for the electrical signal in both RX and TX. When the bias voltage is increased, the total capacitance increases due to a reduced gap height, which, in turn, lowers the upper corner frequency.

The finite size of the device could explain the lower cut-off. The transmission efficiency is reduced at frequencies where the wavelength approaches or exceeds the device size. If the radiation impedance seen by the transducer is real (the element size is much larger than the ultrasonic wavelength in the operation frequency range of the device) and equal to the acoustical impedance of the medium, the Q factor of the membrane defines the low-frequency cut-off. The Q-factor in collapsed operation is higher than that in pre-collapse operation. However, the Q value was small (around 0.1 or smaller) for all CMUTs that we tested, both in pre-collapse and in collapse operation. Therefore, the lower cut-off frequency was mainly affected by diffraction due to the finite device size. Since the element size was the same for the collapsed and pre-collapse CMUT, the low frequency cut-offs were only slightly different in both cases.

Also, since all of the tested devices were equisized, this effect should be the same for all test devices in the dif-

ferent operation modes. Because the device performance in both TX and RX is defined by the average membrane velocity, the cut-off frequency is also affected by the equivalent spring constant of the membrane at the lower end of the bandwidth. At low frequencies, the membrane velocity is linearly proportional to f/k_e where f is the frequency and k_e is the equivalent spring constant of the membrane. Because of a reduction in membrane size in the collapse region, the equivalent spring constant increased with increasing bias voltage as did the low-frequency cut-off, consult Fig. 12 (left). This increase may explain why the FBW remained relatively constant when the bias was increased in the collapse region, since both low-frequency and high-frequency cut-offs increased with the bias voltage.

The mechanisms involved in generating nonlinear distortion in the output signal, Fig. 13, are complex, and a quantitative study of these mechanisms was not pursued. Qualitatively, two contributing mechanisms were identified. In immersion, the impedance of the liquid medium was higher than the impedance of the CMUT membrane within the transducer bandwidth. Thus, the average displacement of a CMUT membrane in both TX and RX was dominated by the bulk properties of the immersion medium, causing the membrane displacement x to be small compared to the average gap d between two electrodes of the devices. Therefore, the nonlinear distortion of both the emitted and the received signals could be obtained from the ratio of the linear term to the second-order term in the Taylor expansion of the relationship between the membrane displacement (x/d) and the electrostatic force in RX, or output pressure in TX, around the bias point. Since the linear term was proportional to (x/d) and the second-order term was proportional to $(x/d)^2$, the latter term increased faster with increased bias voltage than the former term; the same was true for the ratio of the two terms, i.e., the nonlinear distortion as we defined it. Therefore, collapsed region operation—where d was reduced and x was increased due to a stronger electric field compared to conventional region operation—suffered from a higher nonlinear distortion than the conventional operation, Fig. 13.

The nonlinear distortion in TX changed less with bias in collapsed region operation than in conventional region operation. A contribution to the nonlinear distortion in TX, which is proportional to the ratio of the amplitude of the AC signal to the DC bias voltage, arose from the quadratic relationship between electrostatic pressure and applied electric signal [8]. The DC effect was seen as a negative slope in the nonlinear distortion curve for low bias voltages in Fig. 13; the AC effect was seen indirectly as a bending of the graph in Fig. 11, when energy from the fundamental frequency was transferred to higher harmonics [26]. The spectral shape in both TX and in RX is a function of bias voltage, and thus has an impact on f_1/f_0. We argue, however, that since the altered band shape is a desired feature, a comparison can be made between the nonlinear distortion in conventional mode and in collapsed mode operation both in TX and in RX.

While there is evidence that electrostatic effects, e.g., charging, might introduce additional hysteresis to the device function [15], we did not observe charging-dependent hysteresis in this study. The impact of device charging was seen merely as a translation of the bias voltage scale, with no clear impact on the hysteretic behavior of the transducer operating in either region. Charging must be treated with respect, however, since it may cause loss of repeatability in the device performance. Multiple devices were used in order to try to avoid the charging effect.

Hysteresis is a repeatable—but still undesired—feature in an ultrasound imaging transducer. Despite the apparent absence of charge-induced hysteresis, there are at least two other possible mechanisms that could induce the kinds of hysteretic behavior encountered when the CMUTs were operated in collapsed region.

One, with its origin in the collapse and snapback of a membrane [14], [15], [28], depends on the material properties of the membrane and geometry of the unit cell, and was evident as different collapse and snapback voltages, Figs. 6 (left) and 8 (left). Both the collapse and the snapback events are known to be repeatable in the same manner as was evident in this investigation, Figs. 6 (left) and 8 (left). As observed above, with a single crystal membrane, collapse takes place abruptly, whereas snapback takes place in stages [15]. This kind of gradual snapback was not evident in this study, which would indicate that the surface contact during collapse plays an important role in deciding the hysteretic behavior of the CMUT.

Another mechanism known to cause hysteresis in the device behavior is nonuniform adhesion between the membrane face and the bottom electrode along the membrane surface. Surface forces are not readily characterized, however, and are known to be difficult to reproduce in MEMS structures. Adhesion and adhesion hysteresis (changes in adhesion over time) are important factors determining device reliability. The coefficient of variation in adhesion experiments is known to be large, indicating nonuniformity in the mechanism that causes adhesion increase [28].

Since our experimental LVM data (not shown) indicated that identical membranes exhibited different adhesion behavior (especially when the bias voltage was increased), it is likely that the adhesion behavior also caused changes along the membrane surface, e.g., in the contact area, due to micro voids. With increased bias voltage, a higher compression may have altered the surface characteristics, and thus altered the contact area, as compared to a situation where less compression was present. Finally, it is noteworthy that adhesion in a dynamic situation is not identical to adhesion during a static situation. We are currently investigating ways to reduce the hysteresis in the devices by using a differently structured unit cell.

VI. Conclusion

We verified experimentally that collapsed region operation of a CMUT, as predicted by simulations, pro-

vided gains in the transduction efficiency of the transducers greater than CMUT operation in the conventional region. The fractional bandwidth was increased in collapsed region operation, compared to conventional region operation. The devices showed a more pronounced hysteretic behavior when operated in collapsed region than when operated in the conventional region. Reflection measurements showed little difference in reflectivity of the transducer surface when comparing transducer operations in the two regions.

The CMUTs were fabricated by a wafer bonding technique, which produced CMUTs with better control over the gap height than those produced by the traditional sacrificial release process. The 1-D CMUT arrays operating in oil were characterized using ultrasonic pulse-echo and pitch-catch measurements.

Acknowledgment

The authors would like to thank Mr. Utkan Demirci, Dr. G. Göksenin Yaralioglu, and the staff in the Edward L. Ginzton Laboratory at Stanford University for their assistance.

References

[1] A. G. Bashford, D. W. Schindel, and D. A. Hutchins, "Micromachined ultrasonic capacitance transducers for immersion applications," *IEEE Trans. Ultrason., Ferroelect., Freq. Contr.*, vol. 45, pp. 367–375, Mar. 1998.

[2] E. Cianci, V. Foglietti, G. Caliano, and M. Pappalardo, "Micromachined capacitive ultrasonic transducers fabricated using silicon on insulator wafers," *Microelectron. Eng.*, vol. 61–62, pp. 1025–1029, 2002.

[3] P. Eccardt, K. Niederer, T. Scheiter, and C. Hierold, "Micromachined transducers in CMOS technology," in *Proc. IEEE Ultrason. Symp.*, 1996, pp. 959–962.

[4] M. J. Anderson, J. A. Hill, C. M. Fortunko, N. S. Dogan, and R. D. Moore, "Broadband electrostatic transducers: Modeling and experiments," *J. Acoust. Soc. Amer.*, vol. 97, no. 1, pp. 262–272, Jan. 1995.

[5] X. Jin, I. Ladabaum, and B. T. Khuri-Yakub, "The microfabrication of capacitive ultrasonic transducers," *J. Microelectromech. Syst.*, vol. 7, pp. 295–302, Sep. 1998.

[6] Y. Huang, A. S. Ergun, E. Hæggström, M. H. Badi, and B. T. Khuri-Yakub, "Fabricating capacitive micromachined ultrasonic transducers with wafer-bonding technology," *J. Microelectromech. Syst.*, vol. 12, no. 2, pp. 128–137, 2003.

[7] C. G. Oakley and M. J. Zipparo, "Single crystal piezoelectrics: A revolutionary development for transducers," in *Proc. IEEE Ultrason. Symp.*, 2000, pp. 1157–1167.

[8] G. G. Yaralioglu, A. S. Ergun, B. Bayram, E. Hæggström, and B. T. Khuri-Yakub, "Calculation and measurement of electromechanical coupling coefficient of capacitive micromachined ultrasonic transducers," *IEEE Trans. Ultrason., Ferroelect., Freq. Contr.*, vol. 50, no. 4, pp. 449–456, 2003.

[9] A. Bozkurt, I. Ladabaum, A Atalar, and B. T. Khuri-Yakub, "Theory and analysis of electrode size optimization for capacitive microfabricated ultrasonic transducers," *IEEE Trans. Ultrason., Ferroelect., Freq. Contr.*, vol. 46, no. 6, pp. 1364–1374, 1999.

[10] A. S. Ergun, B. Tamelkuran, E. Ozbay, and A. Atalar, "A new detection method for capacitive micromachined ultrasonic transducers," *IEEE Trans. Ultrason., Ferroelect., Freq. Contr.*, vol. 48, no. 4, pp. 932–942, 2001.

[11] M. Kaltenbacher, H. Landes, K. Niederer, and R. Lerch, "3D Simulation of controlled micromachined capacitive ultrasound transducers," in *Proc. IEEE Ultrason. Symp.*, 1999, pp. 1155–1139.

[12] B. Bayram, G. G. Yaralioglu, A. S. Ergun, and B. T. Khuri-Yakub, "Influence of the electrode size and location on the performance of a CMUT [US transducer]," presented at Proc. IEEE Int. Ultrason. Symp., Atlanta, GA, vol. 2, Oct. 7–10, 2001, p. 949–952.

[13] Y. Wang, K. Metzger, D. N. Stephens, G. Williams, S. Brownlie, and M. O'Donnell, "Coded excitation with spectrum inversion (CEXSI) for ultrasound array imaging," *IEEE Trans. Ultrason., Ferroelect., Freq. Contr.*, vol. 50, no. 7, pp. 805–823, 2003.

[14] B. Bayram, E. Hæggström, G. G. Yaralioglu, and B. T. Khuri-Yakub, "A new regime for operating capacitive micromachined ultrasonic transducers," *IEEE Trans. Ultrason., Ferroelect., Freq. Contr.*, vol. 50, no. 9, pp. 1184–1190, 2003.

[15] M. A. Huff, A. D. Nikolich, and M. A. Schmidt, "The threshold pressure switch utilizing plastic deformation of silicon," in *Int. Conf. Solid-State Sens. Actuators, Tech. Dig.*, San Francisco, CA, June 24–27, 1991, pp. 177–180.

[16] A. S. Ergun, G. G. Yaralioglu, and B. T. Khuri-Yakub, "Capacitive micromachined ultrasonic transducers: Theory and technology," *J. Aerospace Eng.*, vol. 16, no. 2, pp. 76–84, 2003.

[17] Y. Huang, A. S. Ergun, E. Hæggström, and B. T. Khuri-Yakub, "Fabrication of capacitive micromachined ultrasonic transducers (CMUTs) using wafer bonding technology for low frequency (10 kHz 150 kHz) sonar applications," presented at IEEE Oceans Conf., Biloxi, MS, vol. 4, Oct. 29–31, 2002, pp. 2322–2327.

[18] Y. Huang, E. Hæggström, B. Bayram, X. Zhuang, A. S. Ergun, C. H. Cheng, and B. T. Khuri-Yakub, "Collapsed region operation of capacitive micromachined ultrasonic transducers based on wafer-bonding technique," presented at Proc. IEEE Int. Ultrason. Symp., Hawaii, 2003.

[19] B. Bayram, G. G. Yaralioglu, E. Hæggström, A. S. Ergun, and B. T. Khuri-Yakub, "Time-dependent ANSYS simulation of water-loaded capacitive micromachined ultrasonic transducer cell in transmission," presented at ANSYS Users Conf. Exhibit., Pittsburgh, May 24–26, 2004.

[20] *ANSYS v. 8 manual*. http://www.ansys.com/services/documentation/manuals.htm.

[21] *Polytec Laser Doppler Vibrometer User Manual*. Tustin, CA: Polytec PI, Inc..

[22] G. S. Kino, *Acoustic Waves: Devices, Imaging, and Analog Signal Processing*. ch. 3, Englewood Cliffs, NJ: Prentice-Hall, 1987.

[23] J. Yamada, "Relation of the insertion loss and the triple transit echo in surface acoustic wave unidirectional transducers," *Ultrasonics*, vol. 40, no. 1–8, pp. 935–937, 2002.

[24] M. P. deBoer, J. A. Knapp, T. M. Mayer, and T. A. Michalske, "The role of interfacial properties on MEMS performance and reliability," in *Proc. SPIE, Int. Soc. Opt. Eng.*, vol. 3825, 1999, pp. 2–15.

[25] O. Oralkan, A. S. Ergun, J. A. Johnson, M. Karaman, U. Demirci, K. Kaviani, T. H. Lee, and B. T. Khuri-Yakub, "Capacitive micromachined ultrasonic transducers: Next-generation arrays for acoustic imaging?," *IEEE Trans. Ultrason., Ferroelect., Freq. Contr.*, vol. 49, no. 11, pp. 1596–1610, 2002.

[26] F. A. Duck, "Nonlinear acoustics in diagnostic ultrasound," *Ultrasound Med. Biol.*, vol. 28, no. 1, pp. 1–18, 2002.

[27] UDV Transducers, http://www.signal-processing.com/tech/us_data_liquid.html, accessed 29 Nov. 2003.

[28] J.-M. Huang, K. M. Liew, C. H. Wong, S. Rajendran, M. J. Tan, and A. Q. Liu, "Mechanical design and optimization of capacitive micromachined switch," *Sens. Actuators A*, vol. 93, no. 3, pp. 273–285, 2001.

Yongli Huang received the B.S. and M.S. degrees in physics from Fudan University in 1987 and 1990, respectively, the M.S. degree in electrical engineering from the University of Hawaii at Manoa in 1996, and the Ph.D. degree in electrical engineering from Stanford University in 2005.

He worked as a Research Associate in the Department of Material Science and Engineering at University of Electronic Science and Technology of China from 1990 to 1992.

He joined SiTek Inc., a subsidiary of BEI Electronics Inc., Campbell, CA, in 1997 as a Member of the Technical Staff and was promoted to a Principal Engineer in 1999. He is currently with Kolo Technologies Inc., San Jose, CA, developing micromachined ultrasonic transducers. His research interests include MEMS technology, sensors and actuators, micromachined ultrasonic devices, inertial sensors, and optical devices.

Edward Hæggström is a visiting scholar at the Ginzton Laboratory (Khuri-Yakub group), Stanford University, CA, on leave from his position as assistant professor at the Department of Physics at the University of Helsinki. He received his D.Sc. degree in 1998 in applied physics from the University of Helsinki, Finland, and an MBA degree in innovation management from the Helsinki University of Technology in 2001. His principal research interests are within ultrasonic characterization of biological samples.

Baris Bayram (S'02) was born in Izmir, Turkey. He received the B.S. degree in 2000 from Bilkent University, Ankara, Turkey, the M.S. degree in 2002 from Stanford University, Stanford, CA, all in electrical engineering. He is currently a Ph.D. candidate in electrical engineering at the E. L. Ginzton Laboratory of Stanford University.

His current research interests include the accurate modeling of capacitive micromachined ultrasonic transducers (CMUTs) using static and dynamic finite element modeling. He particularly investigates the nonlinear operation regimes (collapsed and collapse-snapback) of CMUTs for high performance. He is a student member of the IEEE.

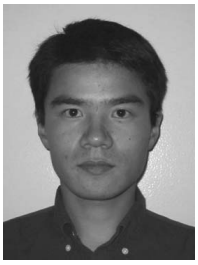

Xuefeng (Steve) Zhuang received the B.S. degree from Louisiana State University, Baton Rouge, LA, in 2002, and the M.S. degree from Stanford University, Stanford, CA, in 2004, both in electrical engineering. He is currently pursuing a Ph.D. degree in electrical engineering at Stanford University. His research interests include the design, fabrication, and packaging of capacitive micromachined ultrasonic transducer arrays, and their integration with medical imaging systems.

A. Sanlı Ergun (S'91–M'99) was born in Ankara, Turkey, in 1969. He received his B.Sc., M.Sc., and Ph.D. degrees in 1991, 1994, and 1999, respectively, all in electrical and electronics engineering from Bilkent University, Ankara, Turkey.

He is now in E. L. Ginzton Laboratory, Stanford University, Stanford, CA, as an engineering research associate. His main research interests are acoustics, ultrasound, microelectromechanical systems (MEMS), and microwave electronics.

Ching-Hsiang Cheng was born in Taipei, Taiwan. He received the B.S. degree in Mechanical Engineering from National Taiwan University in 1993 and the Master's degrees in both Mechanical and Electrical Engineering from Cornell University in 1998. In the same year, he joined Professor Khuri-Yakub's Ultrasonics Group in Electrical Engineering at Stanford University and received his Ph.D. degree in 2005. Following his doctorate degree, he joined Professor Kenneth Goodson's Microscale Heat Transfer Group in Mechanical Engineering, also at Stanford University, as a postdoctoral scholar. After completing his postdoctoral research, he joined Industrial Technology Research Institute (ITRI) in Taiwan as a researcher and become a project leader. In 2006, he was appointed as an Assistant Professor and also a Research Engineer in the Research Institute of Innovative Products and Technologies (RIIPT) of The Hong Kong Polytechnic University. His research interests include electrical through-wafer interconnects, capacitive micromachined ultrasonic transducers (CMUT), microchannels with integrated sensors and actuators, polymeric tactile sensor arrays, nanoimprint technology, and microelectromechanical systems (MEMS) for healthcare applications.

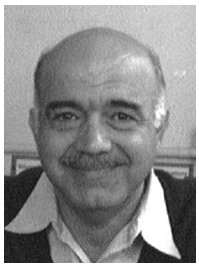

Butrus T. Khuri-Yakub (S'70–S'73–M'76–SM'87–F'95) was born in Beirut, Lebanon. He received the B.S. degree in 1970 from the American University of Beirut, Beirut, Lebanon, the M.S. degree in 1972 from Dartmouth College, Hanover, NH, and the Ph.D. degree in 1975 from Stanford University, Stanford, CA, all in electrical engineering. He joined the research staff at the E. L. Ginzton Laboratory of Stanford University in 1976 as a research associate. He was promoted to a senior research associate in 1978, and to a professor of electrical engineering (research) in 1982. He has served on many university committees in the School of Engineering and the Department of Electrical Engineering.

Presently, he is the Deputy Director of the E. L. Ginzton Laboratory. Dr. Khuri-Yakub has been teaching both at the graduate and undergraduate levels for over 15 years. His current research interests include in situ acoustic sensors (temperature, film thickness, resist cure, etc.) for monitoring and control of integrated circuits manufacturing processes, micromachining silicon to make acoustic materials and devices such as airborne and water immersion ultrasonic transducers and arrays, and fluid ejectors, and in the field of ultrasonic nondestructive evaluation and acoustic imaging and microscopy.

Dr. Khuri-Yakub is a fellow of the IEEE, a senior member of the Acoustical Society of America, and a member of Tau Beta Pi. He is associate editor of *Research in Nondestructive Evaluation*, a journal of the American Society for Nondestructive Testing. He has authored over 400 publications and has been principal inventor or co-inventor of 60 issued patents. He received the Stanford University School of Engineering Distinguished Advisor Award in June 1987 and the Medal of the City of Bordeaux for contributions to nondestructive evaluation, 1983.